iScience

CellPress
OPEN ACCESS

Article

Parvalbumin as a neurochemical marker of the primate optic radiation

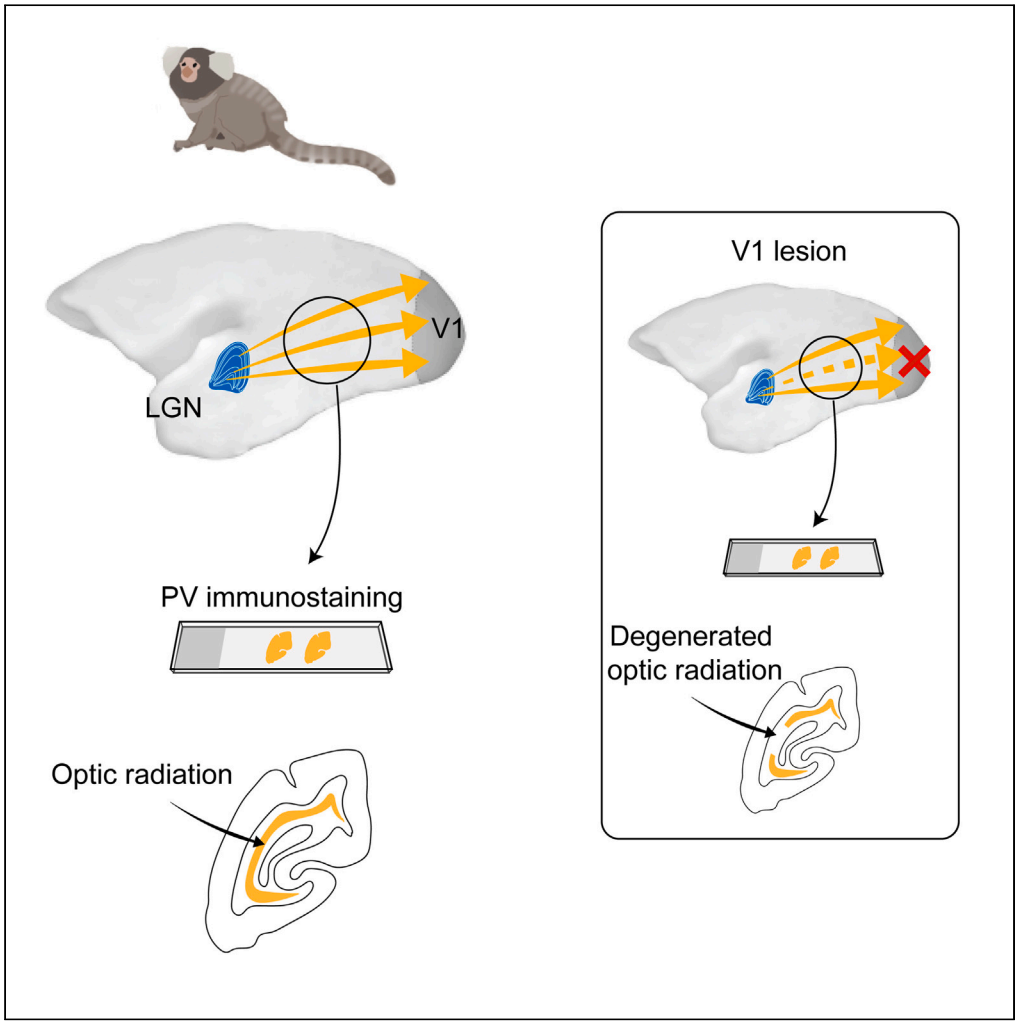

Gaoyuan Ma, Katrina H. Worthy, Cirong Liu, Marcello G.P. Rosa, Nafiseh Atapour

nafiseh.atapour@monash.edu

Highlights

Parvalbumin (PV) immunohistochemistry labels optic radiation (OR) in marmosets

This method identifies OR course in three dimensions with single axon resolution

Primary visual cortex (V1) was the exclusive target for the OR fibers

Degeneration of specific sectors of OR can be mapped following V1 lesions

Ma et al., iScience 26, 106608
May 19, 2023
https://doi.org/10.1016/j.isci.2023.106608

iScience

CellPress
OPEN ACCESS

Article

Parvalbumin as a neurochemical marker of the primate optic radiation

Gaoyuan Ma,[1] Katrina H. Worthy,[1] Cirong Liu,[2] Marcello G.P. Rosa,[1] and Nafiseh Atapour[1,3,*]

SUMMARY

Parvalbumin (PV) is a calcium-binding protein that labels neuronal cell bodies in the magno and parvocellular layers of the primate lateral geniculate nucleus (LGN). Here we demonstrate that PV immunohistochemistry can also be used to trace the optic radiation (OR) of the marmoset monkey (*Callithrix jacchus*) from its LGN origin to its destinations in the primary visual cortex (V1), thus providing a high-resolution method for identification of the OR with single axon resolution. The emergence of fibers from LGN, their entire course and even the entry points to V1 were clearly defined in coronal, parasagittal, and horizontal sections of marmoset brain. In all cases, the trajectory revealed by PV staining paralleled that defined by high-resolution diffusion tensor imaging (DTI). We found that V1 was the exclusive target for the PV-containing fibers, with abrupt transitions in staining observed in the white matter at the border with area V2, and no evidence of PV-labeled axons feeding into other visual areas. Changes in the pattern of PV staining in the OR were detected following V1 lesions, demonstrating that this method can be used to assess the progress of retrograde degeneration of geniculocortical projections. These results suggest a technically simple approach to advance our understanding of a major white matter structure, which provides a cellular resolution suitable for the detection of microstructural variations during development, health and disease. Understanding the relationship between PV staining and DTI in non-human primates may also offer clues for improving the specificity and sensitivity of OR tractography for clinical purposes.

INTRODUCTION

The optic radiation (OR) or geniculocalcarine tract is formed by axons that connect neurons in the lateral geniculate nucleus (LGN) of the thalamus to the primary visual cortex (V1). In primates the OR has long been recognized as a distinctive compartment of the white matter,[1,2] and its damage due to stroke or trauma causes visual deficits in a retinotopic manner.[3–7]

The LGN, which is the origin of OR fibers, contain three main types of geniculostriate projection (or "relay") cells, with the magnocellular (M), parvocellular (P), and koniocellular (K) neurons organized in layers. M and P neurons are known to express calcium-binding protein parvalbumin (PV) while most K neurons, which are interspersed between the other layers, express the calcium-binding protein calbindin (CB).[8–10] Cellular expression of PV is acknowledged as an indicator of a driver function, rather than a modulatory role (the latter being ascribed to thalamic neurons expressing CB).[11–13] These cellular markers are linked to the differential target layers in the V1. While P and M neurons form a large projection ending in layer 4C, K neurons provide a complementary pathway to the V1 that ends on the layers I-III.[14,15] K neurons can also project directly to extrastriate visual cortex.[10,16] In addition to projection neurons there are inhibitory interneurons in the LGN, of which many express PV.[17–19]

PV is a cytosolic protein and thus is known to stain the soma, dendrite, and axons of neurons in a variety of neural structures.[20–22] Here, we present evidence that the OR pathway can be visualized with high-resolution and specificity using a simple immunohistochemical staining for PV. This approach provides a clear map of the three-dimensional course of the OR with single-cell resolution, in a non-human primate brain. Based on examination of both healthy and V1-damaged marmoset monkeys, our results indicate that PV

[1]Neuroscience Program, Biomedicine Discovery Institute and Department of Physiology, Monash University, Clayton, VIC 3800, Australia

[2]Center for Excellence in Brain Science and Intelligence Technology, Institute of Neuroscience, CAS Key Laboratory of Primate Neurobiology, Chinese Academy of Sciences, Shanghai, China

[3]Lead contact

*Correspondence: nafiseh.atapour@monash.edu

https://doi.org/10.1016/j.isci.2023.106608

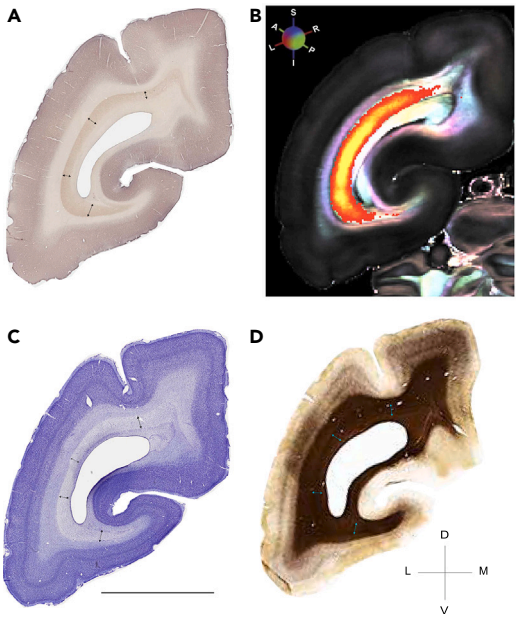

Figure 1. Parvalbumin (PV) stain reveals the optic radiation (OR) with precision

Example images stained for PV (A), Nissl (C) or myelin (D) alongside the directionally encoded color (DEC) map of diffusion tensor (DTI) image (B) in which tractography of the OR is highlighted in the coronal sections (approximately at interaural −0.50 mm[24]). Double-headed arrows in A, C, and D show OR thickness. In DTI image (B), blue, red, and green represent inferior-superior (I-S), left-right (L-R), and anterior-posterior (A-P) white matter fiber direction, respectively. The color of the overlay represents the density of streamlines derived from probabilistic tractography data. Brighter color shows higher density. Scale bar 5 mm. D: dorsal, V: ventral, M: medial, L: lateral.

staining is a suitable approach for the detection of subtle microstructural variations in the primate OR, including those related to disease states.

RESULTS

In PV-stained sections through the posterior part of the marmoset brain, it is possible to distinguish a darker staining compartment in the white matter, which is obvious even at low power (Figures 1 and 2). This compartment is shaped as a folded sheet that surrounds the lateral ventricle. At coronal levels between the caudal end of the thalamus and the rostral end of V1 (Figure 1), this structure occupies approximately the middle third of the white matter depth between the cortex and the ventricle. This level corresponds to the OR identified in the marmoset using DTI[2,23]; see Figure 1B. Examination of adjacent Nissl-stained sections shows a lighter stained compartment of the white matter in a corresponding location (Figure 1C). In comparison, adjacent myelin-stained sections are less informative, as the entire white matter stains darkly; only at higher magnification the OR becomes partially visible (Figure 1D). In comparison with the other techniques (Figure S1), the PV stain reveals the OR consistently and with more precision and greater structural detail (see below). Thus, although the recognition of the OR in Nissl or myelin stain can be achieved, this is best based on the comparison with PV stain.

Similar relationships with DTI images can be visualized in parasagittal and horizontal sections (Figure 2). To enable future study, open-access series of PV-stained sections covering the whole extent of a brain in coronal, sagittal or horizontal planes are provided at Database: https://www.marmosetbrain.org/reference/PV-OR.

Following the OR trajectory in the coronal plane

Figure 3 illustrates a series of coronal sections from rostral to caudal, which shows the changes in the OR trajectory as it approaches V1. The emergence of the OR from the LGN can be visualized in robust detail, with a striking contrast against the surrounding white matter (Figure 3A). It crosses the thalamic reticular nucleus (TRN) in bundles oriented near coronally (Figure 3B), and reaches an intermediate depth between cortex and the TRN (Figure 3C), at that point it becomes widespread mediolaterally. The OR reaches its maximum thickness in the coronal plane around AP levels +4.50 to +2.80 mm relative to the interaural line[24] (Figures 3C and 3D) before becoming thinner and more compressed as it progresses more toward the occipital pole (Figure 3E). At caudal levels the OR surrounds the calcarine sulcus both dorsal and ventrally, and it becomes clear that branches detach from its main body to reach closer to its termination sites (Figure 3E). Cross-sectioned bundles of PV-stained axons are visible in the OR throughout its path as become smaller in size toward the calcarine sulcus (Figure 3). At locations close to V1, the emergence of

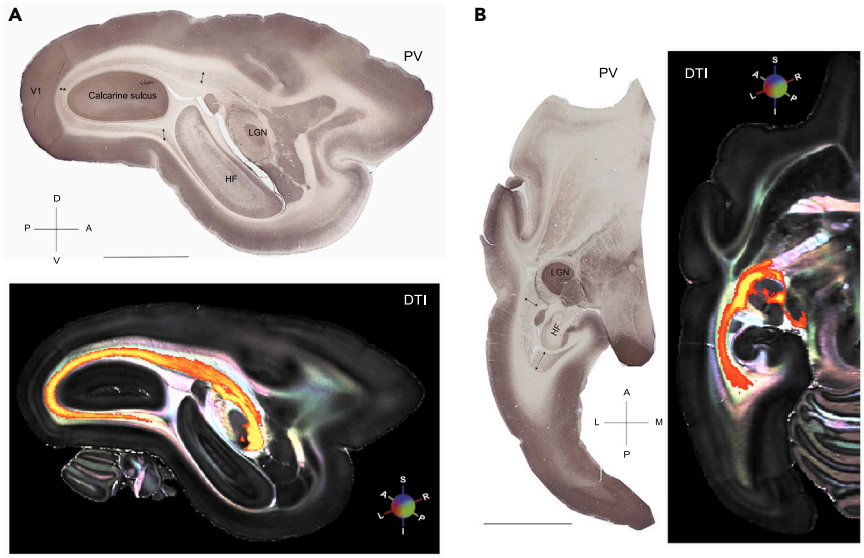

Figure 2. Parvalbumin (PV)-stained area corresponds well with optic radiation (OR) in the corresponding diffusion tensor (DTI) images at sagittal and horizontal planes

The tractography of OR is highlighted in the DTI images. Sagittal plane (A, approximately at +7.00 mm lateral to the midline[25]). Horizontal plane (B, approximately at horizontal −2.36 mm[25]). Double-headed arrows show OR thickness along its route. Dashed lines identify primary visual cortex (V1) border in A. In DTI images, blue, red, and green represent inferior-superior (I-S), left-right (L-R), and anterior-posterior (A-P) white matter fiber direction, respectively. The color of the overlay represents the density of streamlines derived from probabilistic tractography data. Brighter color shows higher density. Scale bar 5 mm. D: dorsal, V: ventral, M: medial, L: lateral, P: posterior & A: anterior. LGN: lateral geniculate nucleus, HF; hippocampal formation.

axons from OR toward V1 can be observed clearly. This pattern of detached fiber bundles was often observed to end abruptly at the border of V1 with the neighboring secondary visual area (V2) (Figures 4A and 4B).

Other visual areas, such as middle temporal area (MT, Figure 4C) are also known to receive LGN input, which however originate in LGN layers where neurons do not stain for PV.[10] Correspondingly, there was no evidence of PV-stained axons detaching from the OR (Figure 4C). These observations indicate that PV staining is an exclusive marker of the components of the OR that feeds into the V1 originating in PV-stained neurons in the magnocellular and parvocellular layers of the LGN.

OR delineation in the sagittal and horizontal planes

Figures 5 and 6 illustrates the trajectory of the OR in parasagittal and horizontal sections of the marmoset brain, respectively. In sections lateral to the calcarine sulcus, the OR occupies a large sector of the central part of white matter (Figure 5A). At this level, it is possible to observe that bundles of OR axons are interspersed with PV-negative bundles, which are likely to contain axons linking other structures or may include fibers originating from non-PV expressing neurons of LGN. At a more medial level (Figure 5B) the emergence of the OR from the LGN can be seen, as well as its pathway toward the posterior pole, which encircles both the calcarine sulcus and the hippocampal formation (Figure 4B). More medial sections (Figures 5C and 5D) reveal both the dorsal and ventral branches of the OR in sharp contrast with other subcomponents of the white matter, as well as detached bundles that approach both the representations of peripheral vision, in the calcarine sulcus, and central vision, in the exposed surface of the occipital pole.[26,27]

In the horizontal plane, emergence of the OR from the LGN and its path encircling the hippocampal formation are well visible in ventral sections (Figures 6A and 6B). Slightly more dorsally, the OR is seen to be connected to a larger portion of LGN, and thus becomes wider as crosses the TRN in bundles (Figure 6B). Similar to observations in the coronal plane, bundles of OR axons are interspersed with PV-negative bundles, which are likely to include fibers originating from non-PV expressing neurons of LGN or other visual

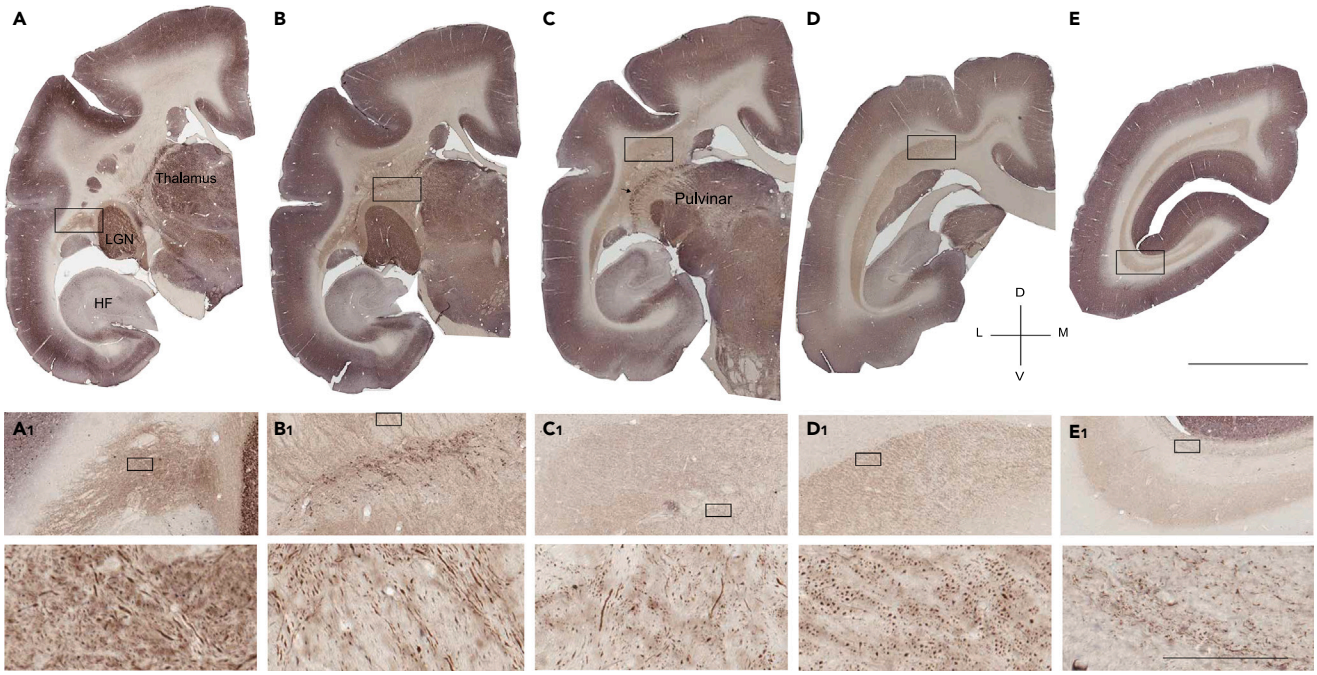

Figure 3. Reliable identification of optic radiation (OR) by parvalbumin (PV) staining throughout its path in the coronal plane

Top: Representative sections at five points along the OR pathway, approximately at interaural +5.00, +4.50, +3.30, +1.80, and −2.50 mm (A–E respectively).[24] Black arrow point to the thalamic reticular nucleus. LGN: lateral geniculate nucleus, HF; hippocampal formation. Scale bar 5 mm. D: dorsal, V: ventral, M: medial & L: lateral. Middle (A1-E1): Magnified black rectangles in A-E. Bottom: magnified black rectangles in A1-E1 indicating PV-stained cross sections of axons through their paths in different directions (scale bar 100 μm).

thalamic nuclei. Further dorsally (Figure 6C), a long cross-section of the OR can be seen, forming an uninterrupted pathway toward V1 and encircling the calcarine sulcus. In a dorsal section, which just grazes through the upper bank of the calcarine sulcus (Figure 5D), the OR occupies almost half of the anterior-posterior dimension toward the occipital pole.

Comparison of axonal staining in the different planes show stained axons cut at different angles (Figures 3, 5 and 6). The majority of axonal cross sections in coronal plane appear as nearly circular profiles, while in the horizontal plane one mostly observes short-length axon fragments running in the direction of the OR. Given the 40 μm thickness, the maximum length of an individual axon captured in a section is approximately 100 μm (Figures 5 and 6).

Evidence of OR degeneration after V1 lesions

Destruction of a portion of V1 leads to retrograde degeneration of neurons in a retinotopically appropriate sector of the LGN, which occurs over a period of months[28–30] and affects primarily projection neurons.[17,30,31] Given this, we investigated the extent to which degenerated sectors of the OR would become evident in the pattern of PV staining 23 months after unilateral lesions, a survival time at which the extent of retrograde degeneration has reached a plateau in the marmoset.[30]

We found that PV staining revealed degenerated sectors of OR. This is evident in Figure 7A by comparing the thickness of the PV-stained sheet in the left (ipsilateral to lesion) and right hemispheres. The degenerated part, characterized by reduced thickness, was restricted to a sector of the OR located lateral to the fundus of the calcarine sulcus (labeled D). In the Nissl stain (Figure 7B) this same sector shows evidence of increased glial scarring, paralleling the increased glial staining in the degenerated sector of the LGN.[10] Close examination shows a near-absence of PV-stained axonal cross sections (Figures 7C–7E). Near the emergence of the OR in the caudal part of the LGN there is an evident gap in white matter PV staining (Figures 7F and 7H between arrows), which again corresponds to a region of glial scarring (Figures 7G and 7I). These results indicate that the marmoset OR is retinotopically organized, with the

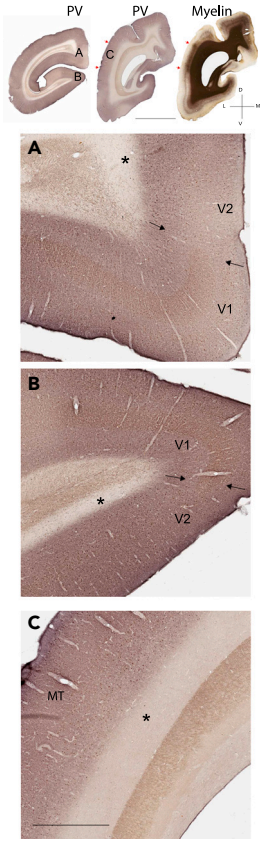

Figure 4. Exclusive entry of optic radiation (OR) fibers into the primary visual cortex (V1)

Top: Representative sections approximately at interaural −4.00 mm (left) and −0.50 mm (middle and right).[24] The heavy myelin stain identifies middle temporal area (MT) located between the two red arrows. Scale bar 5 mm. D: dorsal, V: ventral, M: medial & L: lateral. A-B: The entry of PV-stained axons emerging from OR is shown in high magnification for the two limits of V1. Absence of such fibers is visible in the white matter near the secondary visual area (V2, A,& B) and middle temporal area (MT, C) marked by asterisks. Scale bar 100 μm (A–C).

axons targeting the representation of central vision in V1 running laterally, and demonstrate the feasibility of detecting and quantifying pathological changes restricted to specific sectors of this tract. To further demonstrate the consistent diminished staining along the OR pathway, PV-stained consecutive sections in two-lesioned cases have been shared as open-access datasets (Database: https://www.marmosetbrain.org/reference/PV-OR)

PV-containing fibers other than OR

In sections rostral to the LGN, we observed some PV-stained fibers with trajectories that did not match the DTI-based OR delineations (Figures 3, 5 and 6). It is likely that these represent the axons of PV-expressing projection neurons in other "driver" thalamic nuclei.[20,32–34] Although such axons were also labeled with the present method, their presence did not interfere with the OR delineation. One of these PV-stained fiber bundles was observed in horizontal sections underneath the lateral sulcus and superior temporal gyrus (Figure 6, asterisk in C1), most probably representing PV-containing projection fibers of medial geniculate nucleus reaching to the auditory cortex.[32] The second obvious PV-stained fibers were those present near the somatosensory cortex, presumably originating form somatosensory thalamus.[20,33,34] These fibers can be easily separated from OR based on density of axonal cross sections (Figure 6, dashed line in D).

DISCUSSION

Here we demonstrate a neurochemical identification of a major white matter pathway. We found that immunohistochemical staining for PV labels the axons that collectively form the OR, providing a

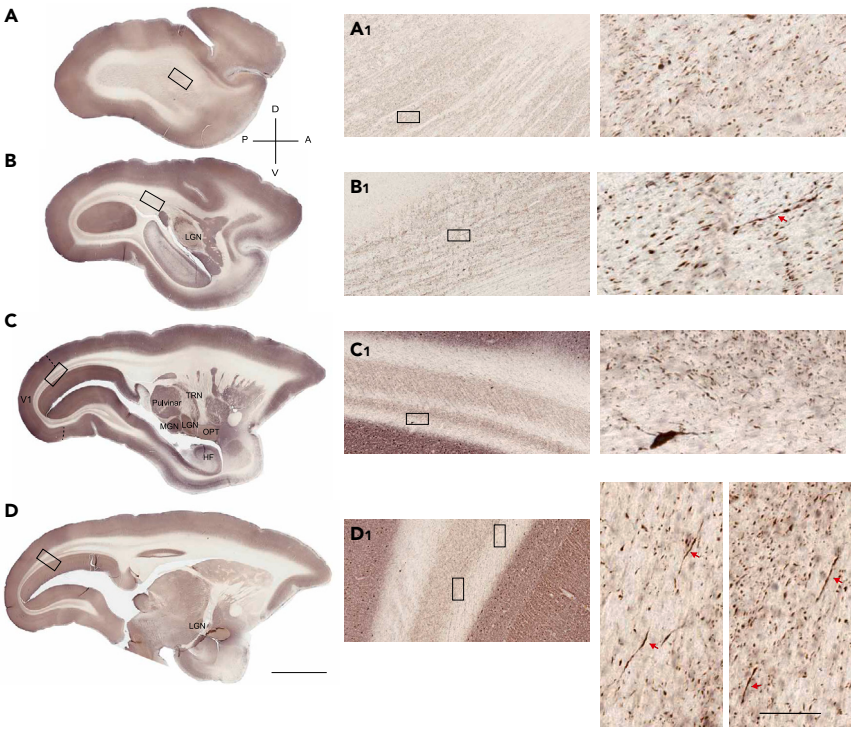

Figure 5. Extent of optic radiation (OR) throughout its path in sagittal sections

Left: Representative sections at four points along the latero-medial direction approximately at +9.00, +7.10, +5.00, and +4.00 mm lateral to the midline.[25] Dashed lines identify primary visual cortex (V1) border in C. Scale bar 5 mm. D: dorsal, V: ventral, P: posterior & A: anterior. Center (A1–D1): Magnified black rectangles in A–D. Right: magnified black rectangles in A1–D1 indicating PV-stained cross sections of axons through their paths in different directions (scale bar 100 μm). Red arrows point to example single axons that run in the direction of the OR. LGN: lateral geniculate nucleus, OPT; optic tract, HF; hippocampal formation, MGN: medial geniculate nucleus, TRN; thalamic reticular nucleus.

high-resolution method for identification of this tract with single axon resolution. We demonstrate the usefulness of this method in neuropathological analysis by providing an example of a condition in which sector-specific retrograde degeneration of the OR after V1 lesion in marmoset monkeys[30] can be detected by the changes in PV staining.

PV is expressed in the M and P neurons of the LGN,[8–10,35] whose axons form the vast majority, if not the entirety of the OR. We show that long-range axons of these neurons strongly express PV, providing a high-resolution and accurate delineation of this tract. The staining exquisitely shows OR-emerging axons that feed into V1, and stop abruptly at the V1-V2 border. This observation is in line with evidence that LGN innervation of extrastriate areas originates in the koniocellular layers, where neurons do not express PV.[10,14,16,35]

Previous immunocytochemical studies have shown that PV is contained in the axons of many of thalamic cells as they enter the monkey cerebral cortex.[8] Presence of PV-labeled fiber bundles in the OR underlying area 17 of human cortex has also been documented.[36] A differential distribution of PV in neuronal compartments could be behind the strong axonal staining for PV, as it has been shown that the axons of cerebellar Purkinje and basket neurons have much higher levels of PV immunoreactivity (10–20 times higher) than the soma and dendrites.[22]

Significant interest in comprehensive mapping of OR lies in its clinical relevance.[7,37,38] Yet, it has been proposed that this is a difficult pathway to image using tractography-based methods.[39] High-resolution *ex vivo* DTI offers information about the main orientation of fiber bundles, which can be used for visualizing and digitally dissecting the occipital white matter of marmosets, including the OR. However, despite the successful reconstruction of the principal bundle of the OR, the limitations of DTI in resolving fiber crossings

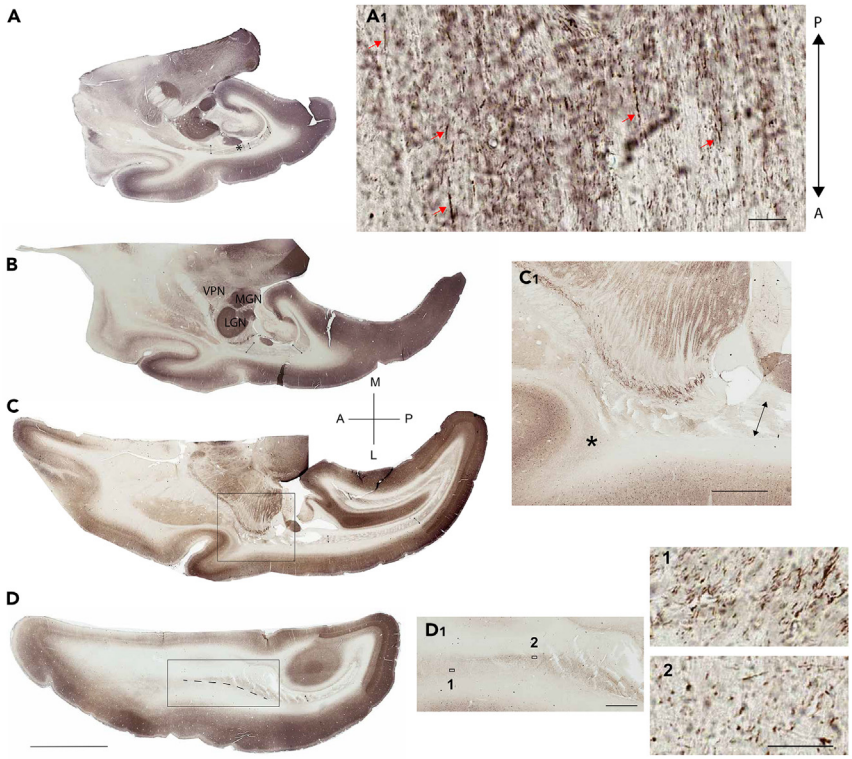

Figure 6. Extent of optic radiation (OR) throughout its path in the horizontal sections

Left: Representative sections at four points (A–D) along the dorsoventral direction approximately at horizontal +7.00, +8.00, +9.30, +13.50 mm, respectively.[25] Dashed line in D separates OR from the other PV-stained fibers. Right: Magnified areas marked by asterisk in A or inside black rectangles in C and D are shown as A1, C1, and D1, respectively. A1: Stained axons run in the direction of the OR. Red arrows point to the longest axons present. C1: Asterisk refers to PV-stained fibers near auditory cortex. D1: For two locations (1 & 2; scale bar 50 μm), PV-stained axonal cross sections are shown. Double-headed arrows point to OR in A-D and C1. M: medial, L: lateral, P: posterior, A: anterior, LGN; lateral geniculate nucleus. MGN: medial geniculate nucleus, VPN: ventral posterior nucleus. Scale bar 5 mm in A-D, 1 mm in C1 and D1, 100 μm in A1.

and terminations have made it difficult to precisely ascertain its full extent. Additionally, the presence of the vertical occipital fasciculus traversing the course of the OR[2] further complicates the full identification of the OR through diffusion tractography. The neurochemical approach suggested here has clear advantages in revealing the full extent of the OR, including its fiber terminations, and may help resolve discrepancies in OR delineations provided by DTI.[40] Machine learning techniques could potentially be used to apply information from the PV-stained sections to DTI images, thereby improving the capacity of DTI to delineate the OR. This principle has the potential to be applied to other species, including humans.

Furthermore, PV-based neurochemical identification of OR combined with other methods could facilitate understanding fine anatomy of this structure. For example, we found that bundles of PV-immunopositive OR axons can be seen interspersed with other axons in the same sectors of white matter (Figure 5), suggesting that the OR shares parts of its trajectory with other neural pathways. Combining PV immunohistochemistry with tracer injections can result in clarification of such relationships, as well as further insights on the fine retinotopic organization. Application of PV immunohistochemistry to a cleared brain, using techniques such as CLARITY,[41] could be used to generate a finer-scale 3D map of this structure. Recently, Nissl-based structure tensor analysis has been used to compare fine-grained features of axonal architecture.[42] Similar quantitative methods are applicable to the PV-stained axons of OR.

Postmortem analysis using PV has the potential to demonstrate the microstructural abnormalities in various white matter diseases, such as multiple sclerosis, Alzheimer disease, leukoencephalopathies, and Wallerian degeneration.[43–45] PV immunostaining may highlight subtle anomalies in the organization of OR,

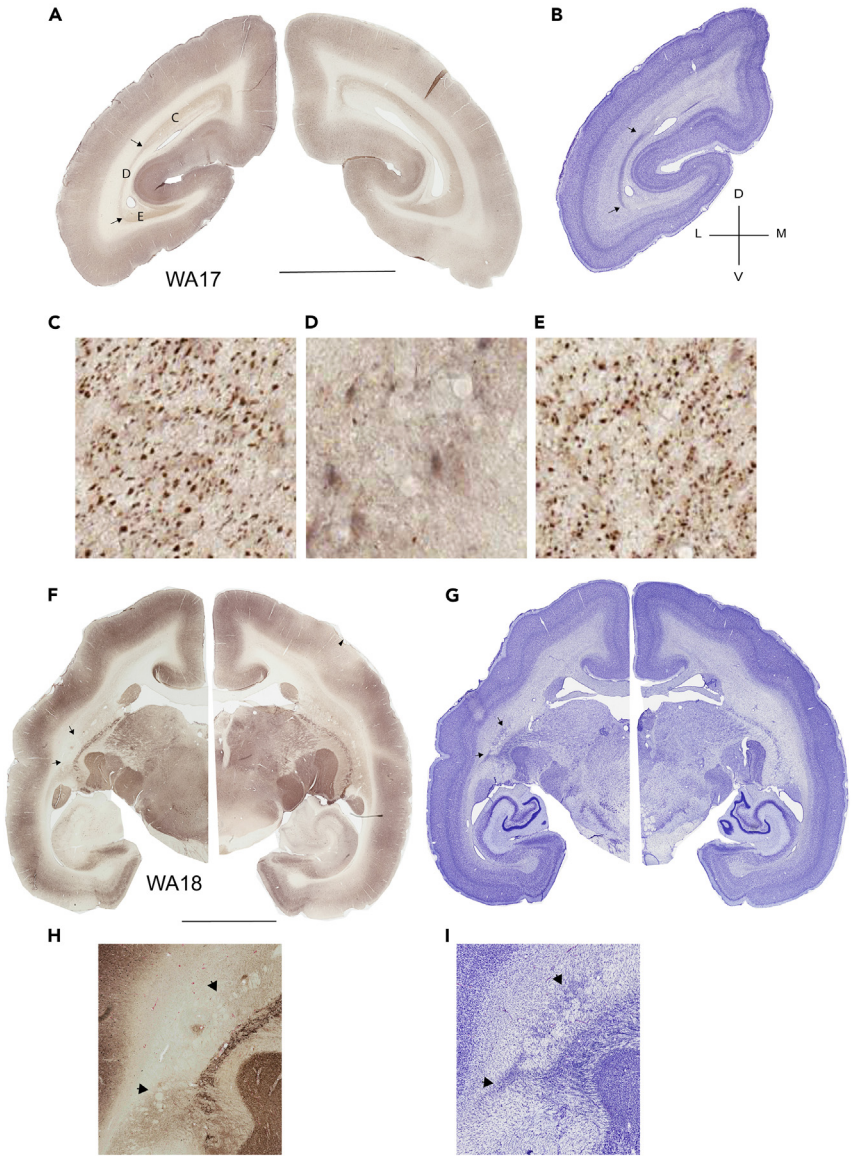

Figure 7. Parvalbumin (PV) staining identifies the degenerated parts of optic radiation (OR) following primary visual cortex (V1) lesion

The degenerated zone in the affected hemisphere (between the two arrows) is shown in the representative sections from two subjects (WA17 and WA18) taken approximately at interaural −0.70 mm (A) and +3.80 mm (F), respectively.[24] Three points along the dorsoventral axis of OR (C–E, 100 × 100 μm^2 each) is shown in higher magnification for WA17. Absence of axonal cross section is clear in D. The degenerated zone is visible in the corresponding Nissl-stained sections (B, G) as a densely stained area. The area between arrows in F and G is shown at higher magnification in H and I, respectively. Scale bar 5 mm. D: dorsal, V: ventral, M: medial & L: lateral.

otherwise not visible purely using anatomical imaging. Furthermore, the single cell axonal resolution provides new quantitative avenues to study plasticity of the white matter in disease conditions that affect primarily central or peripheral vision, such as age-related macular degeneration and glaucoma, which have effects on the central nervous system,[46–48] as well as age- and cognition-related changes.[49]

Staining of axons of additional PV-containing projection neurons originating in other thalamic nuclei,[11,20,32,33] did not impact on the delineation of the OR, as the trajectory of this fiber tract bears a strong compartmentalization in the primate brain. However, our finding suggests that other PV-containing

thalamocortical pathways can also be analyzed in detail using this method, for example following cochlear damage, skin denervation, or amputation.[50,51] PV staining also labels some axonal cross sections in the optic nerve, consistent with expression of PV in some populations of ganglion cells.[52,53] Combining PV staining with other anatomical methods can provide in-depth insights into projection paths in the central nervous system.

In conclusion, the PV-based neurochemical approach to the delineation of OR provides a simple solution to postmortem analysis of this major pathway and extends the potential to the detection of subtle changes in disease states. Comparison of immunohistological delineation of the OR with *in vivo* delineation using neuroimaging may also offer a promising avenue for refinement of tractography, which has significance in the clinical practice of neuro-ophthalmology.

Limitations of the study

This study is reporting the visualization of OR in one species (*Callithrix jacchus*) and future studies is required to test this methodology in other primates including human.

STAR★METHODS

Detailed methods are provided in the online version of this paper and include the following:

- KEY RESOURCES TABLE
- RESOURCE AVAILABILITY
  - Lead contact
  - Materials availability
  - Data and code availability
- EXPERIMENTAL MODEL AND SUBJECT DETAILS
- METHOD DETAILS
  - Tissue processing and immunohistochemistry
  - Probabilistic tractography
- ADDITIONAL RESOURCES
  - Description
  - Supplemental item titles
- QUANTIFICATION AND STATISTICAL ANALYSIS

SUPPLEMENTAL INFORMATION

Supplemental information can be found online at https://doi.org/10.1016/j.isci.2023.106608.

ACKNOWLEDGMENTS

Funding was provided by the National Health and Medical Research Council to Marcello G. P. Rosa (APP1194206) and Nafiseh Atapour (APP2019011) and by the National Natural Science Foundation of China (No. 32171088) and the National Science and Technology Innovation 2030 Major Project of China (No. 2022ZD0205000 and No. 2021ZD0203900) to Cirong Liu. The authors acknowledge the support of the Monash Histology platform, which provided slide scanning services.

AUTHOR CONTRIBUTIONS

N.A. and M.G.P.R. designed the experiments. G.M., K.H.W., N.A., and C.L. performed the experiments. N.A., C.L., and M.G.P.R. wrote the manuscript.

DECLARATION OF INTERESTS

The authors declare there is no conflict of interest.

Received: December 23, 2022
Revised: March 20, 2023
Accepted: March 20, 2023
Published: April 8, 2023

REFERENCES

1. Takemura, H., Pestilli, F., Weiner, K.S., Keliris, G.A., Landi, S.M., Sliwa, J., Ye, F.Q., Barnett, M.A., Leopold, D.A., Freiwald, W.A., et al. (2017). Occipital white matter tracts in human and macaque. Cereb. Cortex *27*, 3346–3359. https://doi.org/10.1093/cercor/bhx070.

2. Kaneko, T., Takemura, H., Pestilli, F., Silva, A.C., Ye, F.Q., and Leopold, D.A. (2020). Spatial organization of occipital white matter tracts in the common marmoset. Brain Struct. Funct. *225*, 1313–1326. https://doi.org/10.1007/s00429-020-02060-3.

3. Ebeling, U., and Reulen, H.J. (1988). Neurosurgical topography of the optic radiation in the temporal lobe. Acta Neurochir. *92*, 29–36. https://doi.org/10.1007/bf01401969.

4. Barton, J.J.S., Hefter, R., Chang, B., Schomer, D., and Drislane, F. (2005). The field defects of anterior temporal lobectomy: a quantitative reassessment of Meyer's loop. Brain *128*, 2123–2133. https://doi.org/10.1093/brain/awh544.

5. Zhang, X., Kedar, S., Lynn, M.J., Newman, N.J., and Biousse, V. (2006). Homonymous hemianopias: clinical-anatomic correlations in 904 cases. Neurology *66*, 906–910. https://doi.org/10.1212/01.wnl.0000203913.12088.93.

6. van Baarsen, K.M., Porro, G.L., and Wittebol-Post, D. (2009). Epilepsy surgery provides new insights in retinotopic organization of optic radiations. A systematic review. Curr. Opin. Ophthalmol. *20*, 490–494. https://doi.org/10.1097/ICU.0b013e3283313c02.

7. Vakharia, V.N., Diehl, B., and Tisdall, M. (2021). Visual field defects in temporal lobe epilepsy surgery. Curr. Opin. Neurol. *34*, 188–196. https://doi.org/10.1097/wco.0000000000000905.

8. Jones, E.G., and Hendry, S.H.C. (1989). Differential calcium binding protein immunoreactivity distinguishes classes of relay neurons in monkey thalamic nuclei. Eur. J. Neurosci. *1*, 222–246. https://doi.org/10.1111/j.1460-9568.1989.tb00791.x.

9. Goodchild, A.K., and Martin, P.R. (1998). The distribution of calcium-binding proteins in the lateral geniculate nucleus and visual cortex of a New World monkey, the marmoset, Callithrix jacchus. Vis. Neurosci. *15*, 625–642. https://doi.org/10.1017/s0952523898154044.

10. Atapour, N., Worthy, K.H., and Rosa, M.G.P. (2022). Remodeling of lateral geniculate nucleus projections to extrastriate area MT following long-term lesions of striate cortex. Proc. Natl. Acad. Sci. USA *119*. e2117137119. https://doi.org/10.1073/pnas.2117137119.

11. Jones, E.G. (2001). The thalamic matrix and thalamocortical synchrony. Trends Neurosci. *24*, 595–601. https://doi.org/10.1016/s0166-2236(00)01922-6.

12. Sherman, S.M. (2007). The thalamus is more than just a relay. Curr. Opin. Neurobiol. *17*, 417–422. https://doi.org/10.1016/j.conb.2007.07.003.

13. Sherman, S.M. (2012). Thalamocortical interactions. Curr. Opin. Neurobiol. *22*, 575–579. https://doi.org/10.1016/j.conb.2012.03.005.

14. Hendry, S.H., and Yoshioka, T. (1994). A neurochemically distinct third channel in the macaque dorsal lateral geniculate nucleus. Science *264*, 575–577. https://doi.org/10.1126/science.8160015.

15. Solomon, S.G. (2002). Striate cortex in dichromatic and trichromatic marmosets: neurochemical compartmentalization and geniculate input. J. Comp. Neurol. *450*, 366–381. https://doi.org/10.1002/cne.10327.

16. Sincich, L.C., Park, K.F., Wohlgemuth, M.J., and Horton, J.C. (2004). Bypassing V1: a direct geniculate input to area MT. Nat. Neurosci. *7*, 1123–1128. https://doi.org/10.1038/nn1318.

17. Atapour, N., Worthy, K.H., and Rosa, M.G.P. (2021). Neurochemical changes in the primate lateral geniculate nucleus following lesions of striate cortex in infancy and adulthood: implications for residual vision and blindsight. Brain Struct. Funct. *226*, 2763–2775. https://doi.org/10.1007/s00429-021-02257-0.

18. Sherman, S.M. (2004). Interneurons and triadic circuitry of the thalamus. Trends Neurosci. *27*, 670–675. https://doi.org/10.1016/j.tins.2004.08.003.

19. Solomon, S.G. (2021). Retinal ganglion cells and the magnocellular, parvocellular, and koniocellular subcortical visual pathways from the eye to the brain. Handb. Clin. Neurol. *178*, 31–50. https://doi.org/10.1016/b978-0-12-821377-3.00018-0.

20. Rausell, E., Bae, C.S., Viñuela, A., Huntley, G.W., and Jones, E.G. (1992). Calbindin and parvalbumin cells in monkey VPL thalamic nucleus: distribution, laminar cortical projections, and relations to spinothalamic terminations. J. Neurosci. *12*, 4088–4111. https://doi.org/10.1523/jneurosci.12-10-04088.1992.

21. DeFelipe, J., Hendry, S.H., and Jones, E.G. (1989). Visualization of chandelier cell axons by parvalbumin immunoreactivity in monkey cerebral cortex. Proc. Natl. Acad. Sci. USA *86*, 2093–2097. https://doi.org/10.1073/pnas.86.6.2093.

22. Kosaka, T., Kosaka, K., Nakayama, T., Hunziker, W., and Heizmann, C.W. (1993). Axons and axon terminals of cerebellar Purkinje cells and basket cells have higher levels of parvalbumin immunoreactivity than somata and dendrites: quantitative analysis by immunogold labeling. Exp. Brain Res. *93*, 483–491. https://doi.org/10.1007/bf00229363.

23. Liu, C., Ye, F.Q., Newman, J.D., Szczupak, D., Tian, X., Yen, C.C.C., Majka, P., Glen, D., Rosa, M.G.P., Leopold, D.A., and Silva, A.C. (2020). A resource for the detailed 3D mapping of white matter pathways in the marmoset brain. Nat. Neurosci. *23*, 271–280. https://doi.org/10.1038/s41593-019-0575-0.

24. Paxinos, G., Watson, C., Petrides, M., Rosa, M.G.P., and Tokuno, H. (2012). The Marmoset Brain in Stereotaxic Coordinates (Academic).

25. Majka, P., Bednarek, S., Chan, J.M., Jermakow, N., Liu, C., Saworska, G., Worthy, K.H., Silva, A.C., Wójcik, D.K., and Rosa, M.G.P. (2021). Histology-based average template of the marmoset cortex with probabilistic localization of cytoarchitectural areas. Neuroimage *226*, 117625. https://doi.org/10.1016/j.neuroimage.2020.117625.

26. Chaplin, T.A., Yu, H.H., and Rosa, M.G.P. (2013). Representation of the visual field in the primary visual area of the marmoset monkey: magnification factors, point-image size, and proportionality to retinal ganglion cell density. J. Comp. Neurol. *521*, 1001–1019. https://doi.org/10.1002/cne.23215.

27. Fritsches, K.A., and Rosa, M.G. (1996). Visuotopic organisation of striate cortex in the marmoset monkey (Callithrix jacchus). J. Comp. Neurol. *372*, 264–282. https://doi.org/10.1002/(sici)1096-9861.

28. Kisvárday, Z.F., Cowey, A., Stoerig, P., and Somogyi, P. (1991). Direct and indirect retinal input into degenerated dorsal lateral geniculate nucleus after striate cortical removal in monkey: implications for residual vision. Exp. Brain Res. *86*, 271–292. https://doi.org/10.1007/bf00228951.

29. Hendrickson, A., Warner, C.E., Possin, D., Huang, J., Kwan, W.C., and Bourne, J.A. (2015). Retrograde transneuronal degeneration in the retina and lateral geniculate nucleus of the V1-lesioned marmoset monkey. Brain Struct. Funct. *220*, 351–360. https://doi.org/10.1007/s00429-013-0659-7.

30. Atapour, N., Worthy, K.H., Lui, L.L., Yu, H.H., and Rosa, M.G.P. (2017). Neuronal degeneration in the dorsal lateral geniculate nucleus following lesions of primary visual cortex: comparison of young adult and geriatric marmoset monkeys. Brain Struct. Funct. *222*, 3283–3293. https://doi.org/10.1007/s00429-017-1404-4.

31. Kinoshita, M., Kato, R., Isa, K., Kobayashi, K., Kobayashi, K., Onoe, H., and Isa, T. (2019). Dissecting the circuit for blindsight to reveal the critical role of pulvinar and superior colliculus. Nat. Commun. *10*, 135. https://doi.org/10.1038/s41467-018-08058-0.

32. Hashikawa, T., Rausell, E., Molinari, M., and Jones, E.G. (1991). Parvalbumin- and calbindin-containing neurons in the monkey medial geniculate complex: differential distribution and cortical layer specific projections. Brain Res. *544*, 335–341. https://doi.org/10.1016/0006-8993(91)90076-8.

33. Rausell, E., and Jones, E.G. (1991). Chemically distinct compartments of the thalamic VPM nucleus in monkeys relay principal and spinal trigeminal pathways to different layers of the somatosensory cortex. J. Neurosci. *11*,

226–237. https://doi.org/10.1523/jneurosci.11-01-00226.1991.

34. Jones, E.G. (1998). Viewpoint: the core and matrix of thalamic organization. Neuroscience *85*, 331–345. https://doi.org/10.1016/s0306-4522(97)00581-2.

35. Yan, Y.H., Winarto, A., Mansjoer, I., and Hendrickson, A. (1996). Parvalbumin, calbindin, and calretinin mark distinct pathways during development of monkey dorsal lateral geniculate nucleus. J. Neurobiol. *31*, 189–209. https://doi.org/10.1002/(SICI)1097-4695.

36. Leuba, G., and Saini, K. (1996). Calcium-binding proteins immunoreactivity in the human subcortical and cortical visual structures. Vis. Neurosci. *13*, 997–1009. https://doi.org/10.1017/s0952523800007665.

37. Yoshida, M., Ida, M., Nguyen, T.H., Iba-Zizen, M.T., Bellinger, L., Stievenart, J.L., Nagao, T., Kikuchi, S., Hara, T., Shiba, T., et al. (2006). Resolution of homonymous visual field loss documented with functional magnetic resonance and diffusion tensor imaging. J. Neuro Ophthalmol. *26*, 11–17. https://doi.org/10.1097/01.wno.0000205620.60510.01.

38. Winston, G.P., Yogarajah, M., Symms, M.R., McEvoy, A.W., Micallef, C., and Duncan, J.S. (2011). Diffusion tensor imaging tractography to visualize the relationship of the optic radiation to epileptogenic lesions prior to neurosurgery. Epilepsia *52*, 1430–1438. https://doi.org/10.1111/j.1528-1167.2011.03088.x.

39. Wu, W., Rigolo, L., O'Donnell, L.J., Norton, I., Shriver, S., and Golby, A.J. (2012). Visual pathway study using in vivo diffusion tensor imaging tractography to complement classic anatomy. Neurosurgery *70*, 145–156. , discussion 156. https://doi.org/10.1227/NEU.0b013e31822efcae.

40. Benjamin, C.F.A., Singh, J.M., Prabhu, S.P., and Warfield, S.K. (2014). Optimization of tractography of the optic radiations. Hum. Brain Mapp. *35*, 683–697. https://doi.org/10.1002/hbm.22204.

41. Chung, K., and Deisseroth, K. (2013). CLARITY for mapping the nervous system. Nat. Methods *10*, 508–513. https://doi.org/10.1038/nmeth.2481.

42. Schurr, R., and Mezer, A.A. (2021). The glial framework reveals white matter fiber architecture in human and primate brains. Science *374*, 762–767. https://doi.org/10.1126/science.abj7960.

43. Pantoni, L., and Garcia, J.H. (1995). The significance of cerebral white matter abnormalities 100 years after Binswanger's report. A review. Stroke *26*, 1293–1301. https://doi.org/10.1161/01.str.26.7.1293.

44. Filley, C.M. (2012). White matter dementia. Ther. Adv. Neurol. Disord. *5*, 267–277. https://doi.org/10.1177/1756285612454323.

45. Chard, D.T., Alahmadi, A.A.S., Audoin, B., Charalambous, T., Enzinger, C., Hulst, H.E., Rocca, M.A., Rovira, À., Sastre-Garriga, J., Schoonheim, M.M., et al. (2021). Mind the gap: from neurons to networks to outcomes in multiple sclerosis. Nat. Rev. Neurol. *17*, 173–184. https://doi.org/10.1038/s41582-020-00439-8.

46. Brown, H.D.H., Woodall, R.L., Kitching, R.E., Baseler, H.A., and Morland, A.B. (2016). Using magnetic resonance imaging to assess visual deficits: a review. Ophthalmic Physiol. Opt. *36*, 240–265. https://doi.org/10.1111/opo.12293.

47. Hanekamp, S., Ćurčić-Blake, B., Caron, B., McPherson, B., Timmer, A., Prins, D., Boucard, C.C., Yoshida, M., Ida, M., Hunt, D., et al. (2021). White matter alterations in glaucoma and monocular blindness differ outside the visual system. Sci. Rep. *11*, 6866. https://doi.org/10.1038/s41598-021-85602-x.

48. Zhuang, J., Madden, D.J., Cunha, P., Badea, A., Davis, S.W., Potter, G.G., Lad, E.M., Cousins, S.W., Chen, N.K., Allen, K., et al. (2021). Cerebral white matter connectivity, cognition, and age-related macular degeneration. Neuroimage. Clin. *30*, 102594. https://doi.org/10.1016/j.nicl.2021.102594.

49. Bells, S., Lefebvre, J., Longoni, G., Narayanan, S., Arnold, D.L., Yeh, E.A., and Mabbott, D.J. (2019). White matter plasticity and maturation in human cognition. Glia *67*, 2020–2037. https://doi.org/10.1002/glia.23661.

50. Rajan, R., Irvine, D.R., Wise, L.Z., and Heil, P. (1993). Effect of unilateral partial cochlear lesions in adult cats on the representation of lesioned and unlesioned cochleas in primary auditory cortex. J. Comp. Neurol. *338*, 17–49. https://doi.org/10.1002/cne.903380104.

51. Jain, N., Florence, S.L., and Kaas, J.H. (1998). Reorganization of somatosensory cortex after nerve and spinal cord injury. News Physiol. Sci. *13*, 143–149. https://doi.org/10.1152/physiologyonline.1998.13.3.143.

52. Kim, T.J., and Jeon, C.J. (2006). Morphological classification of parvalbumin-containing retinal ganglion cells in mouse: single-cell injection after immunocytochemistry. Invest. Ophthalmol. Vis. Sci. *47*, 2757–2764. https://doi.org/10.1167/iovs.05-1442.

53. Hendrickson, A., Yan, Y.H., Erickson, A., Possin, D., and Pow, D. (2007). Expression patterns of calretinin, calbindin and parvalbumin and their colocalization in neurons during development of Macaca monkey retina. Exp. Eye Res. *85*, 587–601. https://doi.org/10.1016/j.exer.2007.07.011.

54. Tournier, J.D., Calamante, F., and Connelly, A. (2012). MRtrix: diffusion tractography in crossing fiber regions. Int. J. Imaging Syst. *22*, 53–66.

55. Rosa, M.G., Tweedale, R., and Elston, G.N. (2000). Visual responses of neurons in the middle temporal area of new world monkeys after lesions of striate cortex. J. Neurosci. *20*, 5552–5563.

56. Gallyas, F. (1979). Silver staining of myelin by means of physical development. Neurol. Res. *1*, 203–209. https://doi.org/10.1080/01616412.1979.11739553.

57. Worthy, K.H., Burman, K.J., and Rosa, M.G.P. (2017). Gallyas Silver Stain for Myelin. Melbourne,Australia: The Marmoset Brain Connectivity Atlas Project. Online. https://doi.org/10.13140/RG.2.2.23807.76968. http://r.marmosetbrain.org/Gallyasmethod.pdf.

58. Veraart, J., Novikov, D.S., Christiaens, D., Ades-Aron, B., Sijbers, J., and Fieremans, E. (2016). Denoising of diffusion MRI using random matrix theory. Neuroimage *142*, 394–406. https://doi.org/10.1016/j.neuroimage.2016.08.016.

59. Jenkinson, M., Beckmann, C.F., Behrens, T.E.J., Woolrich, M.W., and Smith, S.M. (2012). FSL. Neuroimage *62*, 782–790. https://doi.org/10.1016/j.neuroimage.2011.09.015.

STAR★METHODS

KEY RESOURCES TABLE

REAGENT or RESOURCE	SOURCE	IDENTIFIER
Antibodies		
Mouse monoclonal (IgG1) anti-parvalbumin	Swant Inc, Swiss	Code No: 235 RRID: AB_10000343
Biological samples		
Healthy adult marmoset brain	Monash Animal Research platform (MARP)	https://research.monash.edu/en/equipments/animal-research-platform-marp
Marmoset brain with induced lesions of primary visual cortex	Monash Animal Research platform (MARP)	https://research.monash.edu/en/equipments/animal-research-platform-marp
Critical commercial assays		
Biotinylated horse anti-mouse IgG secondary antibody	Vector Laboratories	PK-6102 RRID: AB_2336821
DAB substrate	Vector Laboratories	SK-4100 RRID: AB_2336382
Deposited data		
Parvalbumin immunostaining images across the whole brain	This paper	Database: https://www.marmosetbrain.org/reference/PV-OR
The ultra-high-resolution 80-μm isotropic diffusion MRI	Liu et al.[23]	https://marmosetbrainmapping.org/
Experimental models: Organisms/strains		
Callithrix jacchus	Monash Animal Research platform (MARP)	https://research.monash.edu/en/equipments/animal-research-platform-marp
Software and algorithms		
Aperio ImageScope	Leica Biosystems	https://www.leicabiosystems.com/en-au/digital-pathology/manage/aperio-imagescope/
MRtrix3	Tournier et al.[54]	https://www.mrtrix.org/

RESOURCE AVAILABILITY

Lead contact

Further information and requests for resources and reagents should be directed to and will be fulfilled by the lead contact, Nafiseh Atapour (nafiseh.atapour@monash.edu).

Materials availability

This study did not generate new unique materials.

Data and code availability

- Immunohistochemistry data have been deposited at Database: https://www.marmosetbrain.org/reference/PV-OR and are publicly available as of the date of publication. This data includes images of PV-stained sections of marmoset brain in the coronal, sagittal or horizontal planes.
- No code has been generated in this study.
- Any additional information is available from the lead contact upon request.

EXPERIMENTAL MODEL AND SUBJECT DETAILS

The experiments were conducted in accordance with the Australian Code of Practice for the Care and Use of Animals for Scientific Purposes. All procedures were approved by the Monash University Animal Ethics Experimentation Committee, which also monitored the health and well-being of the animals throughout the experiments. The animals had no veterinary record of serious or chronic health conditions. Materials obtained from five healthy adult marmosets (*C. jacchus*, aged between 32 and 65 months, including four females and one male) and two marmosets (a male and a female) with induced V1 lesions during adulthood. The non-lesioned animals were also used for acute electrophysiological recording experiments not related to the present study. In these cases, the data presented here were obtained from intact hemispheres (i.e., not subject to electrode penetrations). The lesioned animals (WA17 & WA18, aged 56 and 48 months respectively) were both part of previous studies,[10] having survived 23 months after unilateral V1 lesions. The lesion procedures were detailed in these earlier papers. Briefly, under isoflurane anesthesia, an excision was made of all cortical tissue caudal to a plane extending from the dorsal surface of the occipital lobe to the cerebellar tentorium, across the entire mediolateral extent of the left hemisphere.[55] This type of lesion removes the central visual field representation as well as of the peripheral representation up to a minimum of 40° eccentricity along the horizontal meridian[26] corresponding to a minimum of 70% of V1 in one side of the brain. Examples of V1 lesions induced by this method are provided in.[17]

METHOD DETAILS

Tissue processing and immunohistochemistry

At the conclusion of experiments the marmosets were overdosed with pentobarbitone sodium (100 mg/kg) and perfused (either transcardially or through the carotid) with 0.1 M heparinized phosphate buffer (PB; pH 7.2), followed by 4% paraformaldehyde (PFA) in 0.1 M PB. The brains were dissected and post-fixed in the same medium for 24 h, followed by immersion in buffered 4% PFA solutions containing increasing concentrations of sucrose (10%, 20% and 30%). Frozen 40 μm sections in different planes (coronal, parasagittal and horizontal) were obtained using a cryostat, resulting in 5 series. Consecutive sections were stained for Nissl substance using cresyl violet, for myelin (using a variation of the Gallyas[56] stain),[57] and according to different immunostaining procedures (including PV staining)].

For PV staining, the sections were incubated in blocking solution (10% normal horse serum and 0.3% Triton X-100 in 0.1 M PB) for 1 h at room temperature before undergoing primary antibody (PV, 1:8000, Swant Swiss, Code 235, RRID: AB_10000343) incubation at 4°C for 42–46 h. A biotinylated horse anti-mouse IgG secondary antibody (1:200, PK-6102, Vectastain elite ABC HRP kit, Vector Laboratories, RRID: AB_2336821) incubation was then conducted for 30 min - followed by treatment with Avidin-Biotin Complex (ABC) reagent (PK-6102). DAB substrate working solution (DAB kit SK-4100, RRID: AB_2336382) was then applied.

We confirmed that the absence of primary antibody resulted in no staining (Figure S2). Stained sections were scanned using Aperio Scanscope AT Turbo (Leica Biosystems) at ×20 magnification providing a resolution of 0.50 μm/pixel.

Probabilistic tractography

The ultra-high-resolution 80-μm isotropic diffusion MRI data of the Marmoset Brain Mapping Project (marmosetbrainmapping.org) were employed to generate the directionally encoded-color (DEC) map and conduct probabilistic tractography. A comprehensive description of the data is available in our prior publication.[23] The diffusion MRI data were first subjected to denoising via the dwidenoise function implemented in MRtrix3,[58] followed by correction for eddy currents through the application of the eddy_correct function in FSL.[59] The preprocessed data were then fit with the diffusion tensor model using the DTIFIT function in FSL and the multi-shell multi-tissue constrained spherical deconvolution implemented in MRtrix3. These fittings produced fractional anisotropy (FA) maps and FA-weighted DEC maps, as well as fiber orientation distribution (FOD)-weighted images. The DEC map was obtained by multiplying the principal eigenvector (V1) of the diffusion tensor with the FA map generated by DTIFIT. Based on the delineation of Marmoset Brain Mapping Atlas Version 2, the LGN and the V1 label images were extracted and used as the seed and the target images for the tractography. The iFOD2 (Second-order Integration over Fiber Orientation Distributions) method implemented in the "tckgen" command of the software Mrtrix3[54] was performed to generate tracking maps. One million streamlines were selected using the following

parameters: seed_cutoff = 0.1, cutoff = 0.1, maxlength = 25, while the other parameters were kept as default. The tracking results were converted into a density map using "tckmap" commands, which represented the probabilistic map of the OR.

ADDITIONAL RESOURCES

Description

Each folder contains a series of images from marmoset brain sections stained for PV using immunohistochemistry. OR course is visible in the stained sections. Where scanning is purposed for the OR, axonal cross sections are well visible. CJ195, CJ219 and CJ229 represent healthy animals while WA17 and WA18 represent animals with induced lesions of V1.

Coronal plane

Hemisphere/s are cut into caudal (C) and rostral (R) blocks for sectioning, thus sections names containing C and R represent caudal and rostral sections respectively. C1 or R1 represents the most caudal or rostral section respectively. Sections shown in Figures 3A–3E) of the manuscript are R19, R20, C19, C17, C11, respectively.

Horizontal plane

Hemisphere is cut into dorsal (D) and ventral (V) blocks for sectioning, thus sections names containing D and V represent dorsal and ventral sections respectively. D1 or V1 represents the most dorsal and ventral sections, respectively. Sections shown in Figures 6A–6D of the manuscript are V19, V23, V29 and D11, respectively.

Sagittal plane

Hemisphere is cut in the sagittal plane in one block and section S1 represents the most lateral section. Sections shown in Figures 5A–5D of the manuscript are 3, 6, 14 and 19, respectively.

Images are provided in two formats of SVS or JEPG2000 for convenience.

ImageScope viewer of SVS files is available at https://www.leicabiosystems.com/en-au/digital-pathology/manage/aperio-imagescope/

URL:Database: https://www.marmosetbrain.org/reference/PV-OR.

Supplemental item titles

- Measurement of area corresponding to the optic radiation across parvalbumin, Nissl and myelin staining in the coronal plane (Figure S1).
- Absence of anti-parvalbumin primary antibody fails to stain optic radiation (Figure S2).

QUANTIFICATION AND STATISTICAL ANALYSIS

Area corresponding to the OR was measured across PV, Nissl and myelin staining in the coronal plane for one section (Figure S1). No statistical analysis is performed in this study.